ACS APPLIED MATERIALS & INTERFACES

Article

Spatial-Resolved Photoelectrochemical Biosensing Array Based on CdS@g-C3N4 Heterojunction: A Universal Immunosensing Platform for Accurate Detection

Yu-Xiang Dong, Juntao Cao, Bing Wang, Shu-Hui Ma, and Yan Ming Liu

ACS Appl. Mater. Interfaces, **Just Accepted Manuscript** • DOI: 10.1021/acsami.7b13557 • Publication Date (Web): 09 Jan 2018

Just Accepted

ACS Publications

ACS Applied Materials & Interfaces is published by the American Chemical Society.
1155 Sixteenth Street N.W., Washington, DC 20036

Spatial-Resolved Photoelectrochemical Biosensing Array Based on CdS@g-C_3N_4 Heterojunction: A Universal Immunosensing Platform for Accurate Detection

Yu-Xiang Dong, [†,‡] *Jun-Tao Cao,* *[†,‡] *Bing Wang,* [†,‡] *Shu-Hui Ma,* [§] *and Yan-Ming Liu* *[†,‡]

[†]College of Chemistry and Chemical Engineering, Xinyang Normal University, Xinyang 464000, China

[‡]Institute for Conservation and Utilization of Agro-bioresources in Dabie Mountains, Xinyang Normal University, Xinyang 464000, China

[§]Xinyang Central Hospital, Xinyang 464000, China

ABSTRACT: The detection of biomarkers with high sensitivity and accuracy in real biosamples remains challenging. Herein, a universal spatial-resolved photoelectrochemical (PEC) ratiometry for biodetection of prostate specific antigen (PSA) as model biomarker was designed for the first time based on dual-electrodes array modified by CdS@g-C_3N_4 heterojunction coupled with CuS quantum dots (QDs) as signal amplification tags. Specifically, a new kind of photoactive material, CdS@g-C_3N_4 *p-n* heterojunction with highly photoelectric conversion efficiency and good chemical stability, was synthesized and immobilized on two spatial-resolved electrodes (WE1 and WE2). After immobilizing gold nanoparticles, capture PSA antibodies on the electrodes, WE1 incubated with various concentrations of PSA was taken as working electrode, while WE2 with fixed concentration of PSA was used as an internal reference electrode. Next, signal antibodies of PSA labeled CuS QDs as PEC signal quenchers were immobilized on the electrodes to form sandwich-type immunocomplex. With the aid of multiplexed disjunctor, the PEC responses of the dual-electrodes were recorded and PSA was quantified via the ratio values of photocurrent intensity from WE1 to WE2. Combining the fine PEC performance of

CdS@g-C_3N_4 heterojunction with the superior quenching effect of CuS QDs in the spatial resolved platform, the ratiometric system exhibits a linear range from 1.0×10^{-11} to 5.0×10^{-8} g mL^{-1} with the limit of detection of 4.0 pg mL^{-1}. The results demonstrated herein may provide a new pattern for biomarkers detection with high accuracy and good specificity as well as satisfactory applicability in real biosamples.

KEYWORDS: Photoelectrochemical biosensor, spatial-resolved ratiometry, accurate measurement, prostate specific antigen, CdS@g-C_3N_4 heterojunction, CuS quantum dots

1. INTRODUCTION

Photoelectrochemical (PEC) bioassay has attracted great attention in bioanalysis because of its superior merits such as high sensitivity, low background current, simple instrumentation and easy operation.[1-5] Up to now, PEC bioassay has been widely employed to detect various target analytes, including biomarkers, DNA sequences, cancer cells, and metal ions.[6-11] However, in most of the previous methods, the content of target was detected based on one signal change in photocurrent intensity. Such single signal output mode raises the risk of false positive or negative errors due to the fluctuations in photocurrent intensity caused by instrumental or environmental errors, especially in the complex biological samples such as blood and cell samples.[12-14] Therefore, exploring new and more accurate PEC bioanalysis method would be a subject of worthy of study.

As an effective approach to eliminate the interference factors, ratiometric assay which adopts the ratio of two signals rather than absolute value of one signal to achieve the quantification, could effectively normalize the fluctuations caused by the environment variations and offer more accurate detection.[15,16] By far, ratiometry has made rapid progress and developed into many fields, such as electrochemistry (EC), fluorescence, and electrochemiluminescence (ECL).[17-19] For example, based on wavelength-resolved method, a ratiometric fluorescence assay system was performed for sensitive and accurate detection of carboxylesterase.[18] On account of CdS

nanoparticles as cathodic ECL emitter and luminol as anodic ECL emitter, a dual-potentials ECL ratiometry sensing approach for DNA detection was reported.[19]

Great inspirations could be obtained from above examples. It can be predicted that if ratiometry technique is introduced into PEC system, the detection performance might be greatly improved. However, different from the extensive investigation in EC, fluorescence and ECL techniques, studies on ratiometric PEC biosensor are few so far, owing to the difficulty for distinguishing photocurrents from different photoactive materials in a cyclic voltammetry process originated from the inherent mechanism of PEC technique.[12] For example, a wavelength-resolved ratiometric PEC technique for accurate detection of Cu^{2+} in human hair sample was developed using CdS quantum dots and methylene blue with separated absorbance peaks as photoactive models.[15] For construction such PEC sensors, wavelength-selective photoactive materials are crucial and the detection needs a continuous spectrum irradiation for the two PEC active materials to produce two resolved photocurrent, which could not be adopted in general PEC instruments. Recently, by virtue of the potentiometric resolved photocurrents generated from different PEC active materials, Wang's group reported a ratiometric PEC aptasensor for Ochratoxin A detection.[12] However, the requirement of two photoactive materials with different photocurrent polarities at 0 V applied potential to generate distinguishable photocurrent response would limit the widespread application of this kind of PEC biosensor. To overcome these drawbacks, the development of novel ratiometric PEC method, which is not highly depended on the wavelength or potentiometric resolved photoactive materials, is highly desirable.

Most recently, taking advantages of spatial-resolved dual working electrodes, a ratiometric ECL aptasensor for antibiotic chloramphenicol detection was developed based on the ratio of two signals from working electrode and internal reference electrode.[20] In their another report, with the aid of a multiplexed switch, two groups of dual-signals from two spatial-resolved electrodes were employed as dual-signals ratiometric readout for near-simultaneously detecting microRNA-21 and microRNA-141.[21] Inspired by the spatial-resolved ratiometric ECL biosensor, we

speculated that the spatial-resolved PEC ratiometry might possess more attractive analytical performances. However, the performance of PEC biosensor relies heavily on the photoactive materials. To date, various photoactive materials such as TiO_2, CdS, CdSe, and BiOI have been extensively investigated in the construction of PEC biosensors. Among these materials, CdS benefited by its narrow bandgap (2.4 eV) and steerable morphology has attracted great attentions in PEC sensing filed.[22,23] However, the inherent drawback of photocorrosion problem makes CdS unsuitable for its cyclic operation and large scale application. To improve the ability of antiphotocorrosion and PEC activity of CdS, integrating a proper cocatalyst with CdS to form heterojunction is an effective strategy.[24,25] Graphitic carbon nitrides (g-C_3N_4) with relatively low band gap (2.7 eV), suitable band-edge position, and high chemical stability has been used for the fabrication of heterojunction composites semiconductors, such as C_3N_4/TiO_2, C_3N_4/BiOI, $C_3N_4/CoTiO_3$.[26-31] Such heterojunctions have been witnessed their desirable performances and proper stability. Taking into consideration of the above aspects, it can be deduced that judiciously designed heterostructures consisting of CdS and g-C_3N_4 would provide a kind of new and efficient photoactive materials to construct the PEC biosensor.

Herein, a spatial-resolved ratiometric PEC platform for detecting prostate specific antigen (PSA) as model analyte was developed for the first time based on CdS@g-C_3N_4 heterojunction combined with signal amplification probe of CuS conjugated antibodies (Ab_2-CuS). The PEC immunosensing platform was constructed by assembly of CdS@g-C_3N_4, chitosan (CS), gold nanoparticles (AuNPs), Ab_1 on dual-electrodes and then blocking unbound sites with bovine serum albumin (BSA). After adding varied concentration of PSA on WE1 and fixed concentration of PSA on WE2, the equal amount of Ab_2-CuS were incubated onto WE1 and WE2, respectively. The specific immunoreaction between PSA and Ab_2-CuS conjugates results in a noticeably weakened photocurrent response. The spatial-resolved ratiometry was realized on the basis of the ratio of photocurrent intensity between WE1 (providing the working signal) and WE2 (providing the internal reference standard signal), as

shown in scheme 1. By self-calibration of two output signal, the proposed biosensor shows outstanding performance of high accuracy, good selectivity and satisfied applicability in real biosamples.

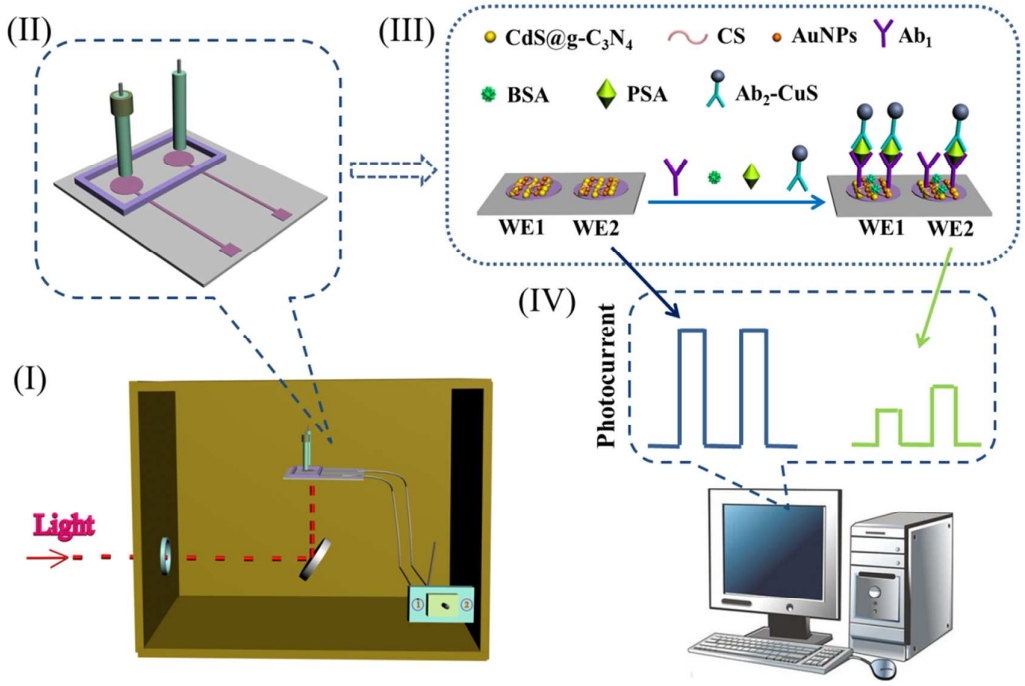

Scheme 1. Schematic illustration of four parts: (I) light path of the device; (II) design of dual-electrodes array; (III) construction of the immunosensor; (IV) the feature of PEC signal.

2. EXPERIMENTAL SECTION

2.1 Preparation of Core-Shell CdS@g-C_3N_4 Nanocomposites. CdS nanoparticles were prepared following the previous report.[32] In brief, 0.64 g of $Cd(CH_3COO)_2$ and 1.82 g of thiourea were added into 60 mL water and mixed well under stirring for 0.5 h. Subsequently, the mixture was put into Teflon-lined autoclave and kept for 5 h under 200 °C. After cooling to room temperature, the obtained yellow sediment was centrifuged, washed by water and ethanol for several times. The CdS nanoparticles were obtained after drying in a vacuum oven.

Water-dispersible g-C_3N_4 was prepared as below:[33] 5 g melamine in crucible was annealed at 550 °C for 4 h. Then 1 g of as-prepared bulk-C_3N_4 powder was refluxed

in 100 mL of 5 M HNO_3 at 125 °C for 12 h and kept overnight. The formed light yellow precipitates were isolated by centrifugation and washed with water for several times. Afterward, the final product was dried at 60 °C for further use.

CdS@g-C_3N_4 nanocomposites were synthesized via self-assembly procedure. In brief, 25 mL of methanol and a measured amount of g-C_3N_4 were added into 50 mL beaker. After treating the mixture under ultrasonic condition for 0.5 h, CdS nanospheres were added into the mixture and kept for stirring for 24 h. Subsequently, the resulting solution was centrifuged and dried at 60 °C under vacuum condition. Following the procedure, a series of the CdS@g-C_3N_4 nanocomposites were prepared by adjusting the weight ratios of g-C_3N_4 to CdS (0, 2, 4, 6, and 8 *wt* %). The samples obtained were labeled as CN0 (pristine CdS), CN2, CN4, CN6, CN8, respectively.

2.2 Preparation of CuS QDs and Ab_2-CuS Conjugates. CuS QDs were synthesized by using thioglycolic acid (TGA) as the capping agent.[34] Briefly, 6.0 μL of TGA was pipetted into 20 mL of 2.0 mM $Cu(NO_3)_2$ aqueous solution and pH was regulated to 9.0. After being bubbled with N_2 for 0.5 h, 5.0 mM Na_2S was added into the mixture. The resulted solution was allowed for reaction for 24 h under N_2 protection. The obtained dark brown colloid solution was centrifuged, washed with ethanol and water, recentrifuged, and finally redispersed in water to form CuS QDs aqueous solution.

Ab_2-CuS conjugates were prepared as below: 200 μL EDC (20 mg mL^{-1}) and NHS (10 mg mL^{-1}) were mingled with 1.0 mL of newly prepared CuS suspension (0.2 mg mL^{-1}) for 0.5 h at room temperature. The mixture was centrifuged to remove the supernatant liquid. After that, 10 μL Ab_2 (2.2 mg mL^{-1}) was mixed and incubated at 4 °C for 12 h under shaking. After being washed with PBS, the acquired bioconjugate was redispersed in 1.0 mL PBS containing 1% BSA.

2.3 Design and Fabrication of Dual-Electrodes. In this work, we have reconstructed the light path and designed the dual-electrodes array. Briefly, a piece of ITO was firstly cut into small slices (4.0 cm × 4.0 cm) and cleaned by putting it into a boiled isopropanol solution containing 2.0 M KOH for 10 min. The ITO working electrodes were fabricated by traditional photolithography method. At length, ITO glasses coated

with positive photoresist were exposed to UV radiation under a mask with the designed micropatterns. After washing and drying at room temperature, the glass was developed by 0.7% NaOH. Then these etched ITO glasses were carried out in the solution of HNO_3: HCl: H_2O = 1:9:10 (volume ratio) for 45 min at 37 °C. After that, the ITO electrodes with the designed patterns were obtained. The PDMS slab with rectangle opening was cast on these glasses by plasma cleaner for 120 s to serve as detection reservoir. Ultimately, the prepared electrodes were rinsed with water and ethanol for future use.

2.4 Construction of the Immunosensor. Firstly, the ITO dual-electrodes were treated with ethanol/water mixture (1:1, *v/v*). Then, 20 μL of 1.0 mg mL^{-1} CdS@g-C_3N_4 was spread onto the surface of two working electrodes with a circular area of 0.1256 cm^2. After being dried, 20 μL of 0.1 mg mL^{-1} CS was dropped onto the CdS@g-C_3N_4 modified electrodes. To avoid the falling of CdS@g-C_3N_4, the modified electrodes were dried at 60 °C. Next, 20 μL of AuNPs were dropped on the resulting electrodes. During this process, AuNPs were immobilized onto the CS-modified ITO through the interaction between -NH_3^+ and AuNPs. Subsequently, 20 μL Ab_1 with a concentration of 200 mg mL^{-1} was immobilized onto the dual-electrode by Au-S bond and incubated at 4 °C for 12 h. After being rinsed with PBS, the electrodes were incubated with 0.1% BSA at 37 °C for 1 h, followed by rinsing with PBS thoroughly. For PSA detection, different concentrations of PSA (1.0×10^{-12} – 1.0×10^{-7} mg mL^{-1}) and fixed concentration of PSA (1.0×10^{-9} mg mL^{-1}) with the same volumes were dropped onto the WE1 and WE2, respectively. After specific immunoreaction between Ab_1 and PSA, the two working electrodes were incubated with 20 μL of Ab_2-CuS conjugates at 37 °C for 1 h. Finally, the electrodes were washed with PBS for the photocurrent measurement.

2.5 Detection Procedure. Before photocurrent test, 500 μL PBS (0.01 M, pH = 7.4) containing 0.1 M AA was injected into the PDMS detection reservoir and the multiplexed switch kept "off". The bias potential was set at 0 V. After that, opening the Xe lamp and turning the switch to the position 1 to connect WE1. 10 s later, the

switch was turned to "off", which was no output of PEC signal. The next 10 s, the switch was converted to the position 2 to connect WE2, and this process was repeated to obtain continuous double PEC signal output. For electrochemical impedance spectroscopy (EIS) detection, the WE2 was covered with non-conductive wall paper. Then, 500 μL of 5.0 mM $K_3[Fe(CN)_6]/K_4[Fe(CN)_6]$ (1:1) containing 0.1 M KCl was injected into the same PDMS modified area. The switch was turned to the position 1 to connect WE1.

3. RESULTS AND DISCUSSION

3.1 Characterizations of CdS@g-C_3N_4 Nanocomposites and AuNPs. SEM and TEM were utilized to acquire the features of CdS, g-C_3N_4 and CdS@g-C_3N_4 heterojunction. The pure g-C_3N_4 with a graphitic-like nanosheet structure could be observed in Figure 1A. The typical SEM image of CdS indicates a uniform morphology and spherical in shape with size of around 250 nm in diameter (Figure 1B). Figure 1C displays the TEM and HRTEM images of pure CdS. As shown in the inset of Figure 1C, the lattice fringes of the pure CdS could be clearly observed and interplanar spacings are estimated to be 0.32 nm, which could be assigned to the (101) plane of CdS.[32] Figure 1D-F are the TEM images of CdS covered with g-C_3N_4 to form a core-shell type nanocomposite. Through TEM observation, it can be seen that C_3N_4 was uniformly attached on the CdS with a thin layer (CN4, Figure 1D) and no distinct morphology changes were observed comparing with pure CdS (Figure 1C). It may be owing to the low loading amount of C_3N_4 on CdS. However, with the amount of g-C_3N_4 increasing, e.g. 8%, the C_3N_4 membrane among CdS nanospheres was formed (Figure 1E). Moreover, the HRTEM images of CdS@g-C_3N_4 composites (Figure 1F) further intuitively demonstrate the formation of heterojunction between CdS and g-C_3N_4.

The crystalline phases and elements composition of the synthesized materials were analyzed by XRD (Figure 1G) and EDS (Figure 1H), respectively. In Figure 1G, the CdS with six distinct diffraction peaks can be identified as the hexagonal wurtzite

structure (JCPDS card no. 75-1545). Two diffraction peaks of pure g-C_3N_4 at 13.2° and 27.4° are corresponded with the (100) and (002) peaks of the graphitic phase, respectively.[35] With the loading of g-C_3N_4, the XRD patterns of CdS@g-C_3N_4 shows no obvious difference compared to the pure CdS, due to the dominance of CdS contribution and low content of g-C_3N_4 (≤ 8% *wt*). The peaks of CdS located at 24.87°, 36.92°, and 47.92° are indexed to (100), (102) and (103) planes, respectively. The existence of the elements of C, N, S and Cd could be observed from the EDS spectrum (Figure 1H), identifying the formation of CdS@g-C_3N_4 composites. In addition, the elemental mapping analysis of CdS@g-C_3N_4 confirmed that the elements of C, N, S and Cd are present in the randomly selected testing area with uniform distribution (as displayed in Figure S1).

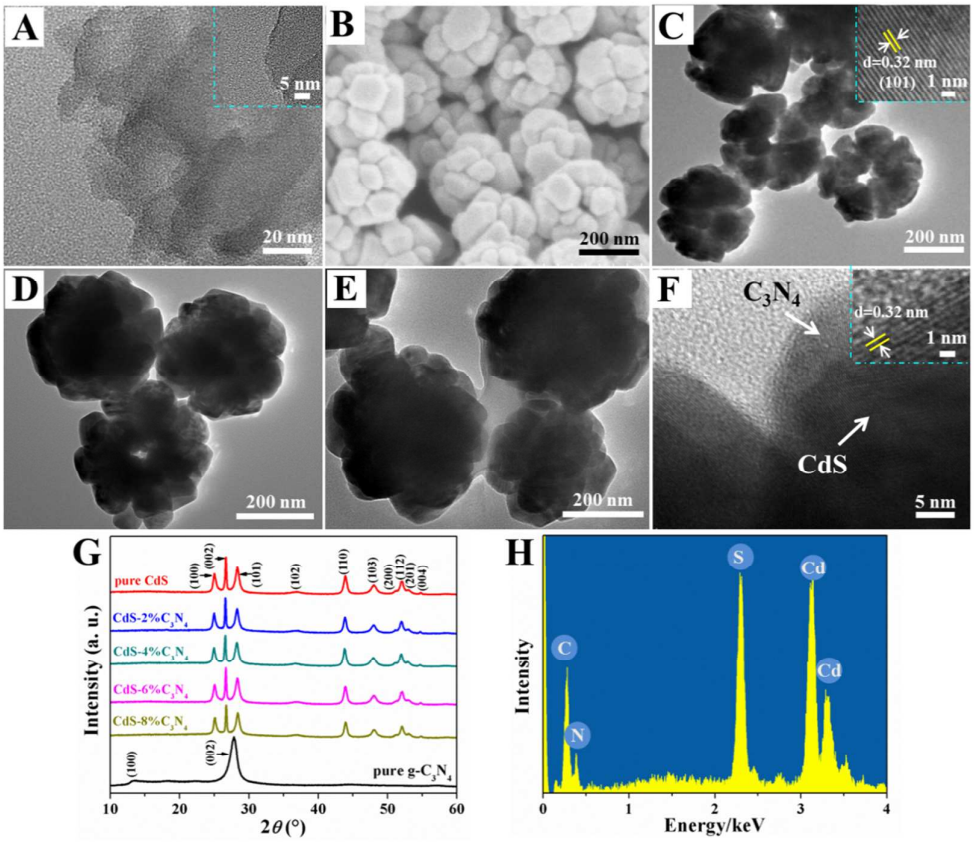

Figure 1. (A) TEM image of g-C_3N_4. Inset: HRTEM image of g-C_3N_4; (B) SEM image of CdS; (C) TEM image of CdS. Inset: HRTEM image of CdS; (D) TEM image of CN4; (E) TEM image of CN8; (F) HRTEM image of CN8; (G) XRD image of CdS, g-C_3N_4 and CdS@g-C_3N_4 composites; (H) EDS image of CdS@g-C_3N_4 composites.

XPS measurements were also performed to confirm the formation of CdS@g-C_3N_4 composites and the XPS spectra of C 1s, N 1s, Cd 3d and S 2p were depicted in Figure 2. In detail, the XPS spectrum of C 1s displays five component peaks (Figure 2A). The peak at 284.9 eV is identified as graphitic carbon (C-C, C=C).[36] The peaks at 285.5, 282.2 and 288.8 eV can be assigned to sp^2 C bonded to N, C bonded with N and sp^2 C bonded to N-containing aromatic structure (N-C=N), respectively.[37] The peak at 289.2 eV is derived from C-OOH bonds.[38] The two peaks at 400.0 and 401.1 eV from the spectrum of N 1s should be interpreted as tertiary nitrogen (N-$(C)_3$) and amino function groups with a hydrogen atom (C-N-H).[39] While the main peaks at 398.9 eV is derived from the sp^2-bonded N in the triazine rings (C-N=C) dominated in g-C_3N_4.[40] In addition, four peaks of 404.9, 411.8, 161.1 and 162.3 eV observed in Cd 3d (Figure 2C) and S 2p (Figure 2D) can be directly assigned to the corresponding species in CdS. Therefore, the formation of CdS@g-C_3N_4 composites can be also confirmed by the XPS.

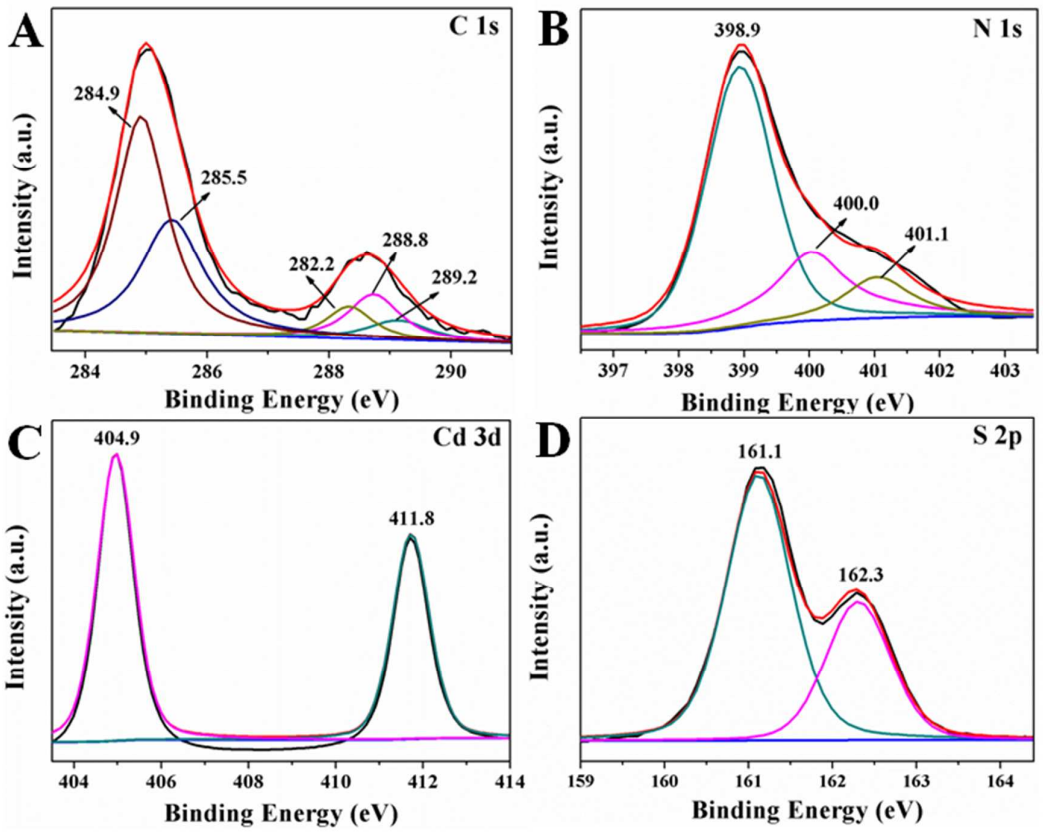

Figure 2. XPS spectra for CdS coated with 8 wt% g-C_3N_4: (A) C 1s; (B) N 1s; (C) Cd

3d; (D) S 2p.

To verify the successful synthesis of AuNPs, TEM and UV–vis absorption spectra were carried out. As can be seen from Figure S2, spherical AuNPs exhibit a highly monodispersion with an average diameter of 15 nm (Figure S2A) and display a strong characteristic absorption band at around 530 nm (Figure S2B).

3.2 Characterization of CuS QDs. Figure 3 shows the TEM image and EDS spectrum of the CuS QDs. From Figure 3A, it can be seen that the synthesized CuS QDs are spherical particles and have a relatively uniform size. The HRTEM image (the inset in Figure 3A) exhibits that the average diameter of CuS QDs is about 4 nm. The EDS spectrum also verified the existence of the elements of Cu and S and the elements of C, O are from -COOH of TGA (Figure 3B). When the CuS QDs were dispersed in water, a homogeneous dark brown solution was obtained (inset of Figure 3B).

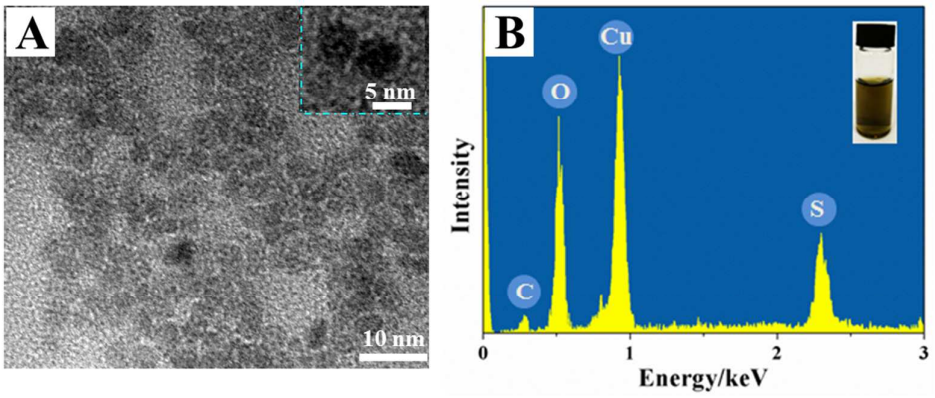

Figure 3. (A) TEM image of CuS QDs. Inset: HRTEM image of CuS QDs; (B) EDS spectrum of CuS QDs. Inset: photograph image of CuS QDs solution.

3.3 PEC Mechanism of the Immunosensor. As shown in Scheme 2, CdS core and g-C_3N_4 shell presented cascade band-edge levels, suggesting that CdS and g-C_3N_4 fulfill the requirement to form heterojunction with well-matched band energies. Under irradiation, different energy gaps of CdS and g-C_3N_4 corresponded to different absorption wavelength, which can sufficiently harvest the exciting light. Besides, because of the matched band-structures and compact contacted interfaces, electron-hole pairs of g-C_3N_4 separated under light induction, and then electrons on

the conduction band (CB) of g-C_3N_4 can directly migrate to the CB of CdS. At the same time, the holes of CdS would transfer to the valence band (VB) of g-C_3N_4. This way greatly promoted the spatial charge separation and increased the photoelectron lifetime as well, resulting in an enhanced photoactivity and stability.

The PSA was detected by constructing a sandwich type PEC immunosensor using Ab_2-CuS conjugates as tags for signal amplification. As signal amplifying elements, Ab_2-CuS conjugates were introduced to effectively weaken the PEC intensity in the presence of PSA, which can be explained as follows: (i) the steric hindrance effect from Ab_2-CuS conjugates impedes AA (electron donor) to the surface of CdS@g-C_3N_4; (ii) under illumination, partially photogenerated electrons from CB of g-C_3N_4 could reversely transfer to CuS due to matched energy band between CuS and g-C_3N_4, leading to reduced photogenerated electrons transfer from CdS@g-C_3N_4 to the electrode;[41] (iii) on account of the wide absorption range of CuS QDs,[42] the light energy to the CdS@g-C_3N_4 could be weakened. Furthermore, the photogenerated electrons on the CuS could be captured by O_2 dissolved in detection solution to form $O_2^{-\bullet}$. Based on the above factors, high sensitivity was conferred to the proposed immunoassay.

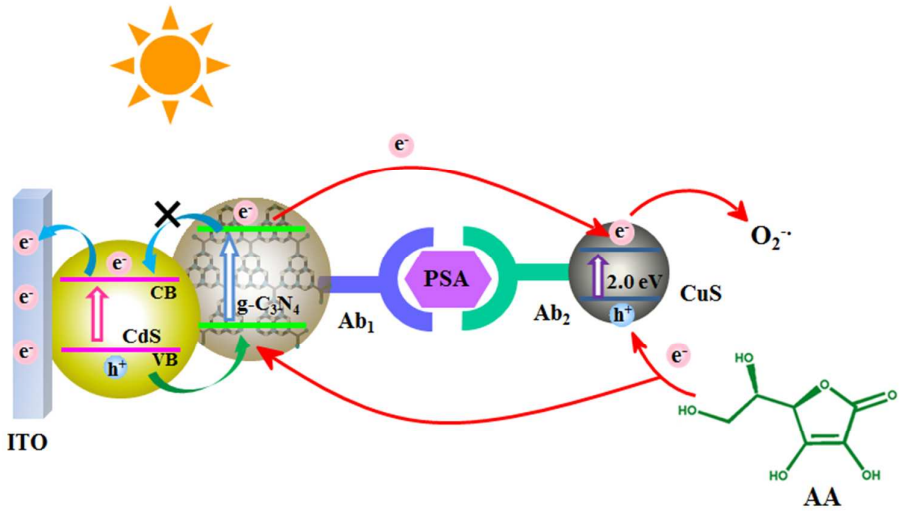

Scheme 2. Charge transfer process of the immunosensor.

3.4 Optimization of Conditions for PEC Detection. The photocurrent responses of the CdS@g-C_3N_4 with different g-C_3N_4 contents were measured. As shown in Figure

S3, the pure g-C_3N_4 (curve a) and CdS (curve b) exhibit a low photocurrent response to light illumination. After CdS was coated with g-C_3N_4 to form CdS@g-C_3N_4 heterojunction, the photocurrent intensity obviously enhanced compared to the pure g-C_3N_4 or CdS. Specifically, the photocurrent intensity of CdS@g-C_3N_4 significantly increased with the thickness of g-C_3N_4 shell increasing (CN2 to CN4), meaning that the coated g-C_3N_4 can effectively promote the charge separation. However, when the weight ratio of g-C_3N_4 to CdS exceeds 4%, the photocurrent decreased (CN6 to CN8). This decrease is mainly because the excessive amount of weak conductivity g-C_3N_4 would block shift of the photogenerated electron. Therefore, CN4 was used for PEC detection.

3.5 EIS and PEC Characterization. EIS is a powerful tool to characterize the fabrication process of the immunosensor. Figure 4A displays the impedance spectra of the electrodes in each construction step on WE1. For bare ITO electrode, the impedance spectrum presented a small R_{et} (curve a). When the CdS@g-C_3N_4, CS, AuNPs, Ab_1 and BSA were assembled on the electrode step by step, the R_{et} increased gradually due to weak conductivity of CdS@g-C_3N_4, hindrance effect of CS, and insulating property of Ab_1 and BSA (curves b-d). After PSA and Ab_2-CuS conjugates were immobilized on the electrode sequentially, the R_{et} enhanced (curves e and f), implying the occurrence of the immunoreaction. Accordingly, the EIS characterizations indicate the successful construction of the immunosensor.

The fabrication process can also be verified by the PEC measurements. As depicted in Figure 4B, the bare ITO electrode shows no photocurrent response (curve a). With the modification process, CdS@g-C_3N_4 modified electrodes gives a great enhanced photocurrent response, which shows good PEC performance of CdS@g-C_3N_4 heterojunction (curve b). After CS, AuNPs, Ab_1 and BSA were incubated on the dual-electrodes, the photocurrent response decreased progressively (curve c and d) because of the poor charge-transfer abilities of CS and steric hindrance effect from the proteins. Subsequently, the as-prepared dual-electrodes immunosensor were incubated with PSA (curve e) and the photocurrent decreased further. From curve e, it also could

be found that the photocurrent intensity of as-prepared working electrode (WE1) was slightly lower than that of internal reference electrode (WE2), as a result of different concentration of PSA modifications on the two electrodes. While the prepared sensing dual-electrodes were incubated with Ab_2-CuS conjugates, the photocurrent intensity further decreased obviously, owing to the efficient quenching effect of Ab_2-CuS conjugates to the photoelectrode (curve f). It is worth noting that decrement of photocurrent intensity of WE1 with 1.0×10^{-7} g mL^{-1} PSA is noticeable compared with that of WE2 with 1.0×10^{-9} g mL^{-1} PSA, demonstrating excellent signal amplification effect of Ab_2-CuS conjugates. Thus, the PEC data also substantiates the successful assembly of the proposed biosensor.

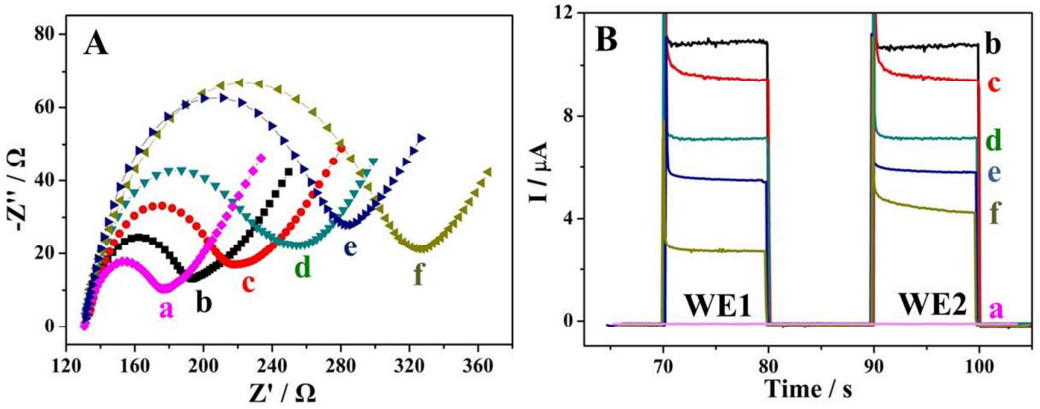

Figure 4. EIS (A) and photocurrent response (B) of electrodes at different stages of (a) bare ITO, (b) after CdS@g-C_3N_4 immobilization, (c) after CS, AuNPs and Ab_1 modification, (d) after incubation with BSA, (e) after incubation with 20 μL of 1.0×10^{-7} g mL^{-1} PSA on WE1 and 1.0×10^{-9} g mL^{-1} PSA on WE2, and then further incubation with Ab_2-CuS (f).

3.6 PEC Detection for PSA. Under the optimized conditions, the photocurrent responses of WE1 gradually decreased with the PSA concentration increasing, while the photocurrent responses at WE2 kept constant, generating ratiometric detection of PSA (Figure 5A). The ratio of PEC intensity ($WE1/WE2_{(R)}$) between these two peaks shows a wide linear relationship with the logarithmic concentration of PSA in the range of 1.0×10^{-11} to 5.0×10^{-8} g mL^{-1} with a correlation coefficient of 0.994 (Figure 5B). The linear equation is $I = -1.312 - 0.258 \log C_{PSA}$ (g mL^{-1}). The limit of

detection for PSA is 4.0 pg mL^{-1}, which is comparable or lower than some previous reports (Table 1), indicating that the developed ratiometric assay exhibits a fine performance for PSA detection.

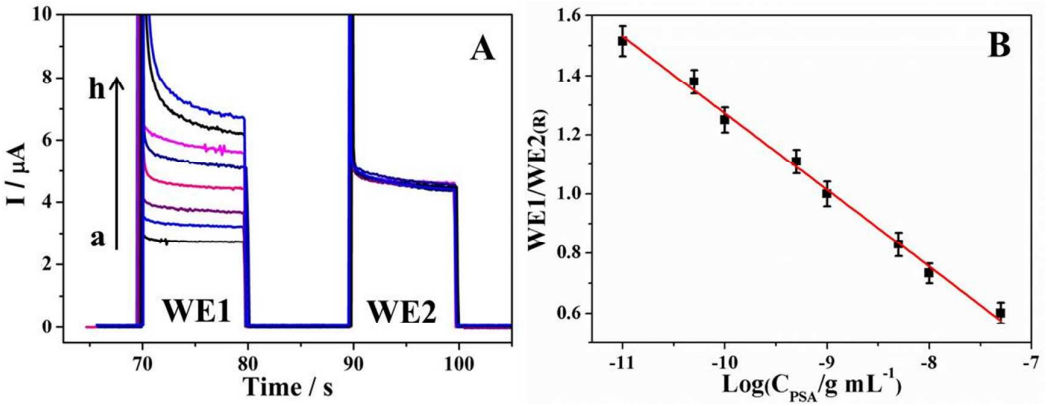

Figure 5. (A) Photocurrent responses of the immunosensor toward varied concentrations of PSA at: (a) 50, (b) 10, (c) 5.0, (d) 1.0, (e) 0.5, (f) 0.1, (g) 0.05, (h) 0.01 ng mL^{-1} on WE1 and 1.0 ng mL^{-1} of PSA on WE2; (B) the linear relationship of the ratio of PEC signal ($WE1/WE2_{(R)}$) with the concentration of PSA (n = 3).

Table 1. Analytical performance of diverse methods to detect PSA

Methods	Linear ranges (ng mL^{-1})	Detection limits (pg mL^{-1})	References
Electrochemistry	0.5 – 40	200	43
Fluorescence	0.1 – 100	27	44
Colorimetric and fluorescence	0.9 – 60	80	45
Electrochemiluminescence	0.5 – 40	100	46
PEC	0.01 – 20	3.8	47
PEC	0.01 – 50	4.0	This work

3.7 Selectivity, Precision and Stability of the Immunosensor. To validate the specificity of the prepared immunoassay, some typical interfering proteins such as HSA and IgG were selected for the test. It can be observed in Figure S4A that photocurrent responses of the interfering proteins are very close to the blank test. In addition, the photocurrent response to the mixed sample containing 40 mg mL^{-1} HSA, 20 mg mL^{-1} hIgG and 0.1 ng mL^{-1} PSA was also studied, and there was no evident

difference in comparison with the result obtained in the presence of 0.1 ng mL^{-1} PSA only. These results reveal that the method has a satisfactory specificity for PSA detection.

The precisions of the immunoassay were investigated based on the relative standard deviations (RSDs) for intra-assay and inter-assay. RSDs of intra-assay are 7.2% and 6.8% to 0.1 ng mL^{-1} and 10 ng mL^{-1} PSA, whereas the values for inter-assay are 5.5% and 7.6%, respectively.

The stability of the photocurrent response of the immunosensor was also evaluated. The PEC responses of 12 repeated on/off illumination cycles was recorded in 500 s. Figure S4B shows that the immunosensor displays no obvious change on photocurrent response. After two weeks storage in PBS at 4 □, the PEC immunosensor still offers stable and negligible difference of photocurrent response.

3.8 Applications in Real Biosamples. To verify the feasibility of the present immunosensor, the content of PSA in seven human serum samples were examined. The serum samples were analyzed directly without any pretreatment. As listed in Table S1, the RSDs of the PEC measurements are no more than 8.2% and relative errors between the present method with the reference method used in Xinyang Central Hospital are less than 7.5%, indicating the great potential of the proposed immunosensor for PSA detection in real samples.

4. CONCLUSIONS

A novel spatial-resolved PEC ratiometric platform was demonstrated for the first time for accurate and sensitive detection of PSA as model analyte. The synthesized CdS@g-C_3N_4 heterojunction, a novel species of superior photoactive material, exhibits excellent PEC performance in this system. Ab_2-CuS conjugates could noticeably decrease the photocurrent response of CdS@g-C_3N_4 electrode, leading to signal amplification for target detection. Integrating the photoactive materials with outstanding properties and the signal amplification strategy, the proposed ratiometric PEC immunosensing platform possesses high accuracy. Moreover, thanks to the tactful signal amplification protocol, the biosensor also shows high sensitivity and

good anti-interference ability for biomarker detection. These results not only extend the properties and applications of CdS@g-C_3N_4 heterojunction materials, but also provide a new universal ratiometry pattern for PEC technology in biochemical analysis.

ASSOCIATED CONTENT

Supporting Information

Additional information contains Chemicals and materials, and instrumentation utilized in this work. HRTEM, scanning transmission electron microscopy (STEM) and element mapping image of CdS@g-C_3N_4 heterojunction, Figure S1. TEM and UV–vis absorption spectra of AuNPs, Figure S2. Photocurrent responses of the CdS@g-C_3N_4 with different g-C_3N_4 contents, Figure S3. Selectivity and stability of the biosensor, Figure S4. Application in complex biological samples, Table S1. The material is available free of charge via the Internet at http://pubs.acs.org.

AUTHOR INFORMATION

Corresponding Authors

* E-mail: liuym9518@sina.com

* E-mail: jtcao11@163.com

Notes

The authors declare no competing financial interest.

ACKNOWLEDGEMENTS

We acknowledge the financial support of the National Natural Science Foundation of China (No. 21675136, 21375114 and 21405129), Plan for Scientific Innovation Talent of Henan Province (2017JR0016), Science & Technology Innovation Talents in Universities of Henan Province (18HASTIT003), Funding Scheme for the Young

Backbone Teachers of Higher Education Institutions in Henan Province (2016GGJS-097), and Nanhu Young Scholar Supporting Program of XYNU.

REFERENCES

(1) Zhao, W. W.; Xu, J. J.; Chen, H. Y. Photoelectrochemical Bioanalysis: The State of The Art. *Chem. Soc. Rev*. **2015**, *44*, 729-741.

(2) Zhao, W. W.; Xu, J. J.; Chen, H. Y. Photoelectrochemical DNA Biosensors. *Chem. Rev*. **2014**, *114*, 7421-7441.

(3) Shu, J.; Qiu, Z.; Zhou, Q.; Lin, Y.; Lu, M.; Tang, D. Enzymatic Oxydate-Triggered Self-Illuminated Photoelectrochemical Sensing Platform for Portable Immunoassay Using Digital Multimeter. *Anal. Chem.* **2016**, *88*, 2958-2966.

(4) Shu, J.; Qiu, Z.; Lin, Z.; Cai, G.; Yang, H.; Tang, D. Semiautomated Support Photoelectrochemical Immunosensing Platform for Portable and High-Throughput Immunoassay Based on Au Nanocrystal Decorated Specific Crystal Facets $BiVO_4$ Photoanode. *Anal. Chem.* **2016**, *88*, 12539-12546.

(5) Dong, Y. X.; Cao, J. T.; Liu, Y. M.; Ma, S. H. A Novel Immunosensing Platform for Highly Sensitive Prostate Specific Antigen Detection Based on Dual-Quenching of Photocurrent from CdSe Sensitized TiO_2 Electrode by Gold Nanoparticles Decorated Polydopamine Nanospheres. *Biosens. Bioelectron.* **2017**, *91*, 246-252.

(6) Liu, Y.; Zhang, Y.; Wu, Fan, D.; Pang, X.; Zhang, Y.; Ma, H.; Sun, X.; Wei, Q. Visible-Light Driven Photoelectrochemical Immunosensor for Insulin Detection Based on MWCNTs@SnS_2@CdS Nanocomposites. *Biosens. Bioelectron.* **2016**, *86*, 301-307.

(7) Lin, Y.; Zhou, Q.; Tang, D.; Niessner, R.; Knopp, D. Signal-On Photoelectrochemical Immunoassay for Aflatoxin B_1 Based on Enzymatic Product-Etching MnO_2 Nanosheets for Dissociation of Carbon Dots. *Anal. Chem.* **2017**, *89*, 5637-5645.

(8) Zhuang, J.; Lai, W.; Xu, M.; Zhou, Q.; Tang, D. Plasmonic AuNP/g-C_3N_4 Nanohybrid-Based Photoelectrochemical Sensing Platform for Ultrasensitive Monitoring of Polynucleotide Kinase Activity Accompanying DNAzyme-Catalyzed Precipitation Amplification. *ACS Appl. Mater. Interfaces* **2015**, *7*, 8330-8338.

(9) Zhao, W. W.; Yu, P. P.; Shan, Y.; Wang. J.; Xu, J. J.; Chen, H. Y. Exciton-Plasmon Interactions between CdS Quantum Dots and Ag Nanoparticles in Photoelectrochemical System and Its Biosensing Application. *Anal. Chem.* **201**2, *84*, 5892-5897.

(10) Liu, S.; Cao, H.; Wang, Z.; Tu, W.; Dai, Z. Label-Free Photoelectrochemical Cytosensing via Resonance Energy Transfer Using Gold Nanoparticle-Enhanced Carbon Dots. *Chem. Comm*. **2015**, *51*, 14259-14262.

(11) Li, J.; Tu, W.; Li, H.; Bao, J.; Dai, Z. In situ generated AgBr-enhanced ZnO Nanorod-Based Photoelectrochemical Aptasensing via Layer-by-Layer Assembly. *Chem. Comm*. **2014**, *50*, 2108-2110.

(12) Zhang, Y.; Hao, N.; Zhou, Z.; Hua, R.; Qian, J.; Liu, Q.; Li, H.; Wang, K. A Potentiometric Resolved Ratiometric Photoelectrochemical Aptasensor. *Chem. Comm*. **2017**, *53*, 5810-5813.

(13) Zhou, Q.; Lin, Y.; Shu, J.; Zhang, K.; Yu, Z.; Tang, D. Reduced Graphene Oxide-Functionalized FeOOH for Signal-on Photoelectrochemical Sensing of Prostate-Specific Antigen with Bioresponsive Controlled Release System. *Biosens. Bioelectron.* **2017**, *98*, 15-21.

(14) Lv, S.; Zhang, K.; Lin, Z.; Tang, D. Novel Photoelectrochemical Immunosensor for Disease-Related Protein Assisted by Hemin/G-Quadruplex-Based DNAzyme on Gold Nanoparticles to Enhance Cathodic Photocurrent on *p*-$CuBi_2O_4$ semiconductor. *Biosens. Bioelectron.* **2017**, *96*, 317-323.

(15) Hao, Q.; Shan, X.; Lei, J.; Zang, Y.; Yang, Q.; Ju, H. A Wavelength-Resolved Ratiometric Photoelectrochemical Technique: Design and Sensing Applications. *Chem. Sci*. **2016**, *7*, 774-780.

(16) Liu, M.; Zhao, H.; Quan, X.; Chen, S.; Yu, H. Signal Amplification via Cation Exchange Reaction: an Example in The Ratiometric Fluorescence Probe for Ultrasensitive and Selective Sensing of Cu (II). *Chem. Comm*. **2010**, *46*, 1144-1146.

(17) Xiong, E.; Zhang, X.; Liu, Y.; Zhou, J.; Yu, P.; Li, X.; Chen, J. Ultrasensitive Electrochemical Detection of Nucleic Acids Based on The Dual-Signaling Electrochemical Ratiometric Method and Exonuclease III-Assisted Target Recycling Amplification Strategy. *Anal. Chem.* **2015**, *87*, 7291-7296.

(18) Wu, Y.; Huang, S.; Zeng, F.; Wang, J.; Yu, C.; Huang, J.; Xie, H.; Wu, S. A Ratiometric Fluorescent System for Carboxylesterase Detection with AIE Dots as FRET Donors. *Chem. Comm*. **2015**, *51*, 12791-12794.

(19) Zhang, H. R.; Xu, J. J.; Chen, H. Y. Electrochemiluminescence Ratiometry: A New Approach to DNA Biosensing. *Anal. Chem.* **2013**, *85*, 5321-5325.

(20) Feng, X.; Gan, N.; Lin, S.; Li, T.; Cao, Y.; Hu, F.; Jiang, Q.; Chen, Y. Ratiometric Electrochemiluminescent Aptasensor Array for Antibiotic Based on Internal Standard Method and Spatial-Resolved Technique. *Sens. Actuators, B* **2016**, *226*, 305-311.

(21) Feng, X.; Gan, N.; Zhang, H.; Li, T.; Cao, Y.; Hu, F.; Jiang, Q. Ratiometric Biosensor Array for Multiplexed Detection of MicroRNAs Based on Electrochemiluminescence Coupled with Cyclic Voltammetry. *Biosens. Bioelectron.* **2016**, *75*, 308-314.

(22) Zang, Y.; Lei, J. P.; Hao, Q.; Ju, H. X. "Signal-On" Photoelectrochemical Sensing Strategy Based on Target-Dependent Aptamer Conformational Conversion for Selective Detection of Lead(II) Ion. *ACS Appl. Mater. Interfaces* **2014**, *6*, 15991-15997.

(23) Zhao, W. W.; Ma, Z. Y.; Yu, P. P.; Dong, X. Y.; Xu, J. J.; Chen, H. Y. Highly Sensitive Photoelectrochemical Immunoassay with Enhanced Amplification Using Horseradish Peroxidase Induced Biocatalytic Precipitation on A CdS Quantum Dots Multilayer Electrode. *Anal. Chem.* **2011**, *84*, 917-923.

(24) Wang, C.; Lin, H.; Xu, Z.; Cheng, H.; Zhang, C. One-Step Hydrothermal Synthesis of Flowerlike MoS_2/CdS Heterostructures for Enhanced Visible-Light Photocatalytic Activities. *RSC Adv.* **2015**, *5*, 15621-15626.

(25) Zang, Y.; Lei, J.; Hao, Q.; Ju, H. CdS/MoS_2 Heterojunction-Based Photoelectrochemical DNA Biosensor via Enhanced Chemiluminescence Excitation. *Biosens. Bioelectron.* **2016**, *77*, 557-564.

(26) Cui, W.; Li, J.; Dong, F.; Sun, Y.; Jiang, G.; Cen, W.; Lee, S. C.; Wu, Z. Highly Efficient Performance and Conversion Pathway of Photocatalytic NO Oxidation on SrO-Clusters@Amorphous Carbon Nitride. *Environ. Sci. Technol.* **2017**, *51*, 10682-10690.

(27) Cui, W.; Li, J.; Cen, W.; Sun, Y.; Lee, S. C.; Dong, F. Steering the Interlayer Energy Barrier and Charge Flow via Bioriented Transportation Channels in g-C_3N_4: Enhanced Photocatalysis and Reaction Mechanism. *J. Catal.* **2017**, *352*, 351-360.

(28) Wang, Z.; Guan, W.; Sun, Y.; Dong, F.; Zhou, Y.; Ho, W. K. Water-Assisted Production of Honeycomb-Like g-C_3N_4 with Ultralong Carrier Lifetime and Outstanding Photocatalytic Activity. *Nanoscale* **2015**, *7*, 2471-2479.

(29) Fan, D.; Guo, C.; Ma, H.; Zhao, D.; Li, Y.; Wu, D.; Wei, Q. Facile Fabrication of An Aptasensor for Thrombin Based on Graphitic Carbon Nitride/TiO_2 with High Visible-Light Photoelectrochemical Activity. *Biosens. Bioelectron.* **2016**, *75*, 116-122.

(30) Wang, J. C.; Yao, H. C.; Fan, Z. Y.; Zhang, L.; Wang, J. S.; Zang, S. Q.; Li, Z. J. Indirect Z-Scheme BiOI/g-C_3N_4 Photocatalysts with Enhanced Photoreduction CO_2 Activity Under Visible Light Irradiation. *ACS Appl. Mater. Interfaces* **2016**, *8*, 3765-3775.

(31) Ye, R.; Fang, H.; Zheng, Y. Z.; Li, N.; Wang, Y.; Tao, X. Fabrication of $CoTiO_3$/g-C_3N_4 Hybrid Photocatalysts With Enhanced H_2 Evolution: Z-Scheme Photocatalytic Mechanism Insight. *ACS Appl. Mater. Interfaces* **2016**, *8*, 13879-13889.

(32) Han, S.; Pu, Y. C.; Zheng, L.; Zhang, J. Z.; Fang, X. Shell-Thickness Dependent Electron Transfer and Relaxation in Type-II Core-Shell CdS/TiO_2 Structures with Optimized Photoelectrochemical Performance. *J. Mater. Chem. A* **2015**, *3*, 22627-22635.

(33) Liu, Y.; Yan, K.; Zhang, J. Graphitic Carbon Nitride Sensitized with CdS Quantum Dots for Visible-Light-Driven Photoelectrochemical Aptasensing of Tetracycline. *ACS Appl. Mater. Interfaces* **2015**, *8*, 28255-28264.

(34) Zhu, Y. D.; Peng, J.; Jiang, L. P.; Zhu, J. J. Fluorescent Immunosensor Based on CuS Nanoparticles for Sensitive Detection of Cancer Biomarker. *Analyst* **2014**, *139*, 649-655.

(35) Dong, G.; Zhang, L. Porous Structure Dependent Photoreactivity of Graphitic Carbon Nitride under Visible Light. *J. Mater. Chem.* **2012**, *22*, 1160-1166.

(36) Liu, Y.; Liu, L.; Shan, J.; Zhang, J. Electrodeposition of Palladium and Reduced gGraphene Oxide Nanocomposites on Foam-Nickel Electrode for Electrocatalytic Hydrodechlorination of 4-Chlorophenol. *J. hazard. Mater.* **2015**, *290*, 1-8.

(37) Yan, S. C.; Li, Z. S.; Zou, Z. G. Photodegradation of Rhodamine B and Methyl Orange Over Boron-Doped g-C_3N_4 under Visible Light Irradiation. *Langmuir* **2010**, *26*, 3894-3901.

(38) Hou, Y.; Wen, Z.; Cui, S.; Guo, X.; Chen, J. Constructing 2D Porous Graphitic C_3N_4 Nanosheets/Nitrogen□Doped Graphene/Layered MoS_2 Ternary Nanojunction with Enhanced Photoelectrochemical Activity. *Adv. Mater.* **2013**, *25*, 6291-6297.

(39) Jiang, F.; Yan, T.; Chen, H.; Sun, A.; Xu, C.; Wang, X. A g-C_3N_4-CdS Composite Catalyst with High Visible-Light-Driven Catalytic Activity and Photostability for Methylene Blue Degradation. *Appl. Surf. Sci.* **2014**, *295*, 164-172.

(40) Lu, M.; Pei, Z.; Weng, S.; Feng, W.; Fang, Z.; Zheng, Z.; Huang, M.; Liu, P. Constructing Atomic Layer g-C_3N_4-CdS Nanoheterojunctions with Efficiently Enhanced Visible Light Photocatalytic Activity. *Phys. Chem. Chem. Phys.* **2014**, *16*, 21280-21288.

(41) Liu, Y.; Li, R.; Gao, P.; Zhang, Y.; Ma, H.; Yang, J.; Du, B.; Wei, Q. A Signal-Off Sandwich Photoelectrochemical Immunosensor Using TiO_2 Coupled with CdS as The Photoactive Matrix and Copper (II) Ion as Inhibitor. *Biosens. Bioelectron.* **2015**, *65*, 97-102.

(42) Fan, G. C.; Zhu, H.; Du, D.; Zhang, J. R.; Zhu, J. J.; Lin, Y. H. Enhanced Photoelectrochemical Immunosensing Platform Based on CdSeTe@CdS:Mn Core-Shell Quantum Dots-Sensitized TiO_2 Amplified by CuS Nanocrystals Conjugated Signal Antibodies. *Anal. Chem.* **2016**, *88*, 3392-3399.

(43) Zhao, N.; He, Y.; Mao, X.; Sun, Y.; Zhang, X.; Li, C. Z.; Lin, Y.; Liu, G. Electrochemical Assay of Active Prostate-Specific Antigen (PSA) Using Ferrocene-Functionalized Peptide Probes. *Electrochem. Commun.* **2010**, *12*, 471-474.

(44) Xu, D. D.; Deng, Y. L.; Li, C. Y.; Lin, Y.; Tang, H. W. Metal-Enhanced Fluorescent Dye-Doped Silica Nanoparticles and Magnetic Separation: A Sensitive Platform for One-Step Fluorescence Detection of Prostate Specific Antigen. *Biosens. Bioelectron.* **2017**, *87*, 881-887.

(45) Barbosa, A. I.; Gehlot, P.; Sidapra, K.; Edwards, A. D.; Reis, N. M. Portable Smartphone Quantitation of Prostate Specific Antigen (PSA) in A Fluoropolymer Microfluidic Device. *Biosens. Bioelectron.* **2015**, *70*, 5-14.

(46) Yang, H.; Li, Z.; Shan, M.; Li, C.; Qi, H.; Gao, Q.; Wang, J.; Zhang, C. Electrogenerated Chemiluminescence Biosensing for The Detection of Prostate PC-3 Cancer Cells Incorporating Antibody as Capture Probe and Ruthenium Complex-Labelled Wheat Germ Agglutinin as Signal Probe. *Anal. Chim. acta* **2015**, *863*, 1-8.

(47) Zhang, K.; Lv, S.; Lin, Z.; Tang, D. CdS: Mn Quantum Dot-Functionalized g-C_3N_4 Nanohybrids as Signal-Generation Tags for Photoelectrochemical Immunoassay of Prostate Specific Antigen Coupling DNAzyme Concatamer with Enzymatic Biocatalytic Precipitation. *Biosens. Bioelectron.* **2017**, *95*, 34-40.

Table of Contents Graphic